Int. J. Electrochem. Sci., 17 **(2022)** Article Number: 22058, doi: 10.20964/2022.05.17

International Journal of
ELECTROCHEMICAL
SCIENCE
www.electrochemsci.org

Short Communication

Improved Corrosion Resistance of Surface Mechanical Attrition Treated Tantalum

Hua Li[1], *Zhongjie Wang*[2], *Hua Dai*[3,4], *Yuan Luo*[4], *Hongzhong Cai*[4], *Haijun Wu*[3,4*], *Zhentao Yuan*[1*], *Xiao Wang*[1*]

[1] City College, Kunming University of Science and Technology, Kunming, 650093, China;
[2] School of Materials Science and Engineering, Yancheng Institute of Technology, Yancheng, 224051, China;
[3] School of Materials Science and Engineering, Kunming University of Science and Technology, Kunming, 650093, China;
[4] Kunming Institute of Precious Metals, Kunming, State Key Laboratory of Advanced Technologies for Comprehensive Utilization of Platinum Metals, 650106, China.
[*]E-mail: whj@ipm.com.cn (Haijun Wu), wang_welding@163.com (Xiao Wang), kmust_welding@163.com (Zhentao Yuan)

Received: 21 December 2021 / *Accepted:* 5 Feruary 2022 / *Published:* 5 April 2022

Tantalum (Ta) has been used extensively in high-temperature anti-corrosion applications because of its resistance to almost all strong acids. However, its strong anisotropic corrosion results in service failure of the Ta and restricts its further application in high-technology industries. In this work, surface mechanical attrition treatment (SMAT) followed by anodizing was used to improve the corrosion resistance of Ta materials. The surface morphology and grain size of Ta coatings were studied by scanning electron microscopy and X-ray diffractometry, respectively. The corrosion resistance of Ta oxide films was assessed by electrochemical tests. In addition, the activation mechanism of the Ta surface was investigated by molecular dynamics simulation. The grain size of the Ta surface crystal decreased significantly after SMAT. The grain size on the Ta surface was 13.2 nm for a SMAT of 5 min, whereas X-ray photoelectron spectroscopy depth sputtering showed that the oxide film layer thickness increased by 340% after SMAT. The electrochemical properties of the Ta anodic oxide coating showed that the largely improved corrosion performance was attributed to the enhanced stability of the passivation zone. At the same times, the SMAT for 5 min increased the corrosive potential (–1.143 V_{SCE}) and reduced the corrosion current (1.028 × 10^{-5} A·cm^{-2}). Meanwhile, the molecular dynamics results indicate two orders of magnitude increase in atomic diffusion rate of the nanostructures compared with the non-SMAT Ta surfaces. This study shows that SMAT pretreatment can enhance the corrosion resistance of Ta materials, and extend the service environment and service life of Ta.

Keyword: surface mechanical attrition treatment; corrosion resistance; tantalum

1. INTRODUCTION

The continuous development of aerospace technology has increased requirements for high-temperature material properties that can serve in extreme environments, such as strong corrosion and oxidation [1]. Tantalum (Ta) has been used extensively in high-temperature, anti-corrosion environments because of its resistance to almost all strong acids, except hydrofluoric acid [2]. However, its strong anisotropic corrosion results in service failure of the Ta and reduces its application in high-technology industries [3].

Researchers have conducted extensive research to enhance the corrosion resistance of Ta materials, such as surface anodization, elemental doping modification, and surface activation treatment. Anodic oxidation and process parameter modifications are straightforward, convenient, and applied more often than other approaches. Amsel et al. [4] produced Ta_2O_5 films by the anodic oxidation of Ta in sulfuric-acid electrolyte. Hu et al. [5] demonstrated that the Ta_2O_5 coating enhances the Ti–6Al–4V alloy corrosion resistance significantly. Many studies have shown that doping with elemental Ta enhances the corrosion resistance. Li et al. [6] injected Ta atoms onto the TiNi alloy surface and formed a Ta_2O_5/TiO_2 film with a significantly higher electrochemical impedance. In addition, Vallat et al. [7] used plasma etching to enhance the selective deposition of Ta_2O_5 films and obtained a significantly thicker oxide film. The methodologies above have improved the corrosion resistance of the material surface to various extents, however, the results remain unsatisfactory. The anodic oxide film is thin and has a short service life under extreme service conditions, but elemental doping can lead to the formation of microcells and aggravate corrosion. Furthermore, the surface etching is a complex process that cannot be applied on a large scale. Therefore, the search for a simpler surface activation method to enhance the coating thickness and corrosion resistance has been the focus of scientific researchers.

Surface mechanical attrition treatment (SMAT) is a typical approach to modifying the surface characteristics of materials to decrease the surface grain size to the nanoscale level. Previous studies have confirmed that the SMAT, owing to its large specific surface area, high surface energy, and high surface activity, can enhance the material surface activity. For example, Fu et al. [8] reported on the effects of SMAT on the corrosion behavior of commercial pure titanium, and a comparison of current densities at the same polarized potential showed a significant reduction in dissolution current of the treated sample. Meanwhile, the diffusion behavior of Ti atoms in pure nanocrystalline Fe was investigated [9], as described by a vacancy model, first-principles calculations, and experimentally. The results imply that SMAT can increase the surface vacancy concentration and enhance the atomic diffusion rate, which promotes surface film formation.

To improve the Ta corrosion resistance, SMAT pretreatment was carried out before anodizing Ta. The surface micromorphology after SMAT was analyzed by scanning electron microscopy (SEM). The grain refinement effect was examined by X-ray diffractometry (XRD). The corrosion resistance of Ta was assessed by electrochemical testing and the effect of SMAT treatment on the corrosion resistance of Ta was studied by molecular dynamics.

2. EXPERIMENTAL AND COMPUTATIONAL DETAILS

2.1 Preparation of Ta anodic oxide coatings

The rolled Ta sheet specimen dimensions were 15 mm × 15 mm × 1 mm (Ningxia Oriental Tantalum Industry Co., Ltd., Ningxia, China), and they were vacuum annealed at 800 °C for 1 h. SMAT was performed on annealed specimens with a surface mechanical grinding device as shown in Fig. 1a. Because of the high density of impact of the SiC balls on the specimen surface (the test parameters were SiC spheres with an 8-mm diameter and a vibration frequency of 50 Hz), nanocrystalline layers formed on the material surface.

The principle of surface nanosizing is shown in Fig. 1b. When the spheres impact the surface, they deform the grains compressively near the surface, which results in grain fragmentation and refinement. The degree of refinement on the surface is higher than the degree of refinement on the inside, with an asymptotic increase in the degree of nanosizing as the grinding time is enhanced. The test with 2 and 5 min of mechanical grinding was labelled Ta_{SMAT2} and Ta_{SMAT5}, respectively, compared with Ta without mechanical grinding.

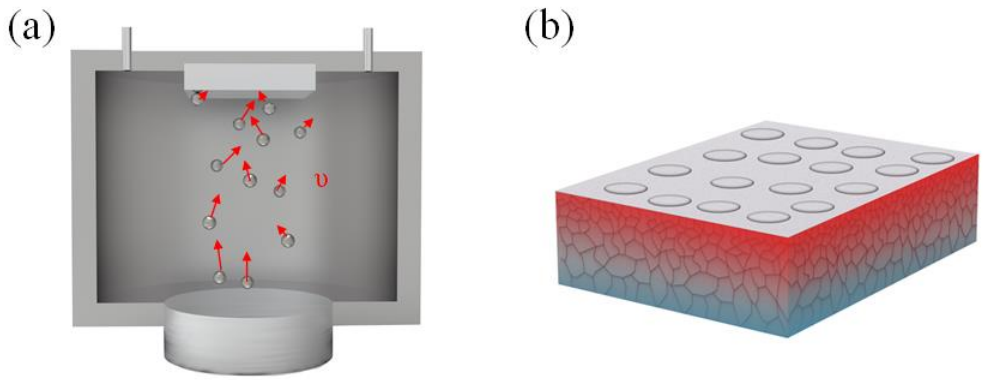

Figure 1. (a) SMAT device, the SiC spheres hit the surface of the specimen above the shaking box with different velocities and directions, and the pipe is a vacuum extraction device. (b) SMAT operating principle, the closer the area to the surface, the smaller the grain size was (red area).

The specimens were degreased by a combination of ultrasonic degreasing with acetone and cathodic degreasing with dilute sulfuric acid. Anodic oxidation was carried out in a conventional two-electrode system with Ti sheets as the anode and graphite plates as the cathode, with a cathode-to-anode plate area ratio of 3:1 and a plate spacing of 5 cm. Before anodic oxidation, high-purity nitrogen was introduced into the electrolyte to remove oxygen that was mixed in the electrolyte. The tests were anodized in a 0.5 M H_2SO_4 solution with 20 V as the anodizing potential, at 25°C and with an anodizing time of 600 s.

2.2 Materials characterization and electrochemical measurements

The surface morphology of the films was obtained by SEM (XL-30Philips, Japan). The phase compositions and average crystallite sizes were determined by XRD with Cu–Kα radiation (tube voltage: 40 kV, tube current: 200 mA for structural analysis). XRD analysis was performed with a scanning speed of 1°/min and a 2θ range of 10–100° for wide-angle XRD patterns.

Electrochemical measurements were performed on a CHI660E electrochemical workstation (CH Instruments, Shanghai). A three-electrode system consisted of a reference electrode (saturated calomel electrode, SCE), counter electrode (Pt sheet), and working electrode (10 mm × 10 mm × 2 mm Ta coating). Electrochemical measurements were tested in 3.5 wt % NaCl solution at room temperature. Potentiodynamic polarization curves were measured from −3.5 V to 7.0 V at 0.5 mV/s. Corrosion parameters, such as the corrosion potential (E_{corr}) and corrosion current density (j_{corr}) were calculated by Tafel extrapolation of the cathodic slope.

2.3 Molecular dynamics simulation

A polycrystalline model was built using Atomsk software, and the structural characteristics were simulated by molecular dynamics simulations using the LAMMPS program. Three configurations were simulated, with particle numbers including one, five, and ten crystals in a 100 nm ×100 nm ×100 nm box. The Ta potential function (Ta.eam/alloy) that was developed by Li et al. [10] was chosen from among the potential functions.

The setup was subjected to a 10 *ps* relaxation at 300 K to bring it as close to thermodynamic equilibrium as possible before the simulation began. The simulations were run in an NPT ensemble with a Nose/Hoover temperature thermostat with $k_BT/K_{Reff} = 10^{-3}$ and a Berendsen pressure barostat during the relaxation. Surfaces were created by deleting atoms in the 6-nm length region of the *c*-axis by using an NPT ensemble. During the run, data on the system temperature, potential energy, and kinetic energy were gathered, and the atoms' root-mean-square displacement was computed at 300 K.

3. RESULTS AND DISCUSSION

3.1 Surface morphology of the Ta coating

Figure 2 shows the SEM image of the Ta plate before and after SMAT. As shown in the figure, the untreated surface was relatively smooth and many cracks were generated on the Ta plate surface after mechanical grinding treatment for 2 and 5 min because of the violent plastic deformation of the Ta surface, which was triggered when the SiC balls repeatedly hit the Ta surface at a high rate. According to Lu et al. [11] surface nanosizing caused the surface to break up after process hardening, which boosted the surface energy and provided more diffusion channels for atomic diffusion. A comparison of the number of surface cracks for various SMAT times showed that the number of cracks after mechanical grinding increased, as the mechanical grinding time increased.

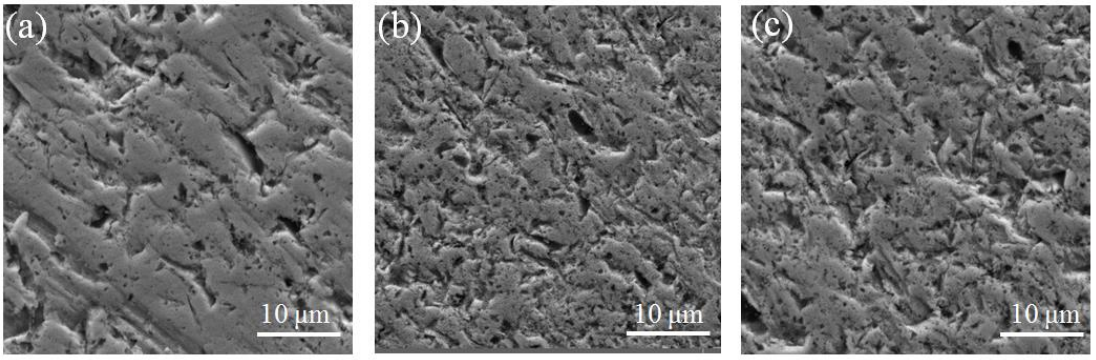

Figure 2. Scanning electron micrographs of Ta surface before and after SMAT (a) Ta, (b) Ta_{SMAT2}, (c) Ta_{SMAT5}. (The dark regions represent nanopores or surface defect, and the gray regions represent substrate)

Figure 3 shows the XRD spectrum of the Ta, Ta_{SMAT2}, and Ta_{SMAT5} samples. It can be seen that the intensity of the diffraction peaks of the Ta_{SMAT2} and Ta_{SMAT5} sample was less than that of the original coarse crystalline sample relative to the untreated Ta sample, with the (200) and (211) and (310) diffraction peaks being broadened significantly. The ease of slip differs from one crystal plane to another because of the different punctuated resistances to dislocation movement of each crystal plane, which resulted in different degrees of broadening of each crystal plane in the XRD diffraction spectrum.

Diffraction peak broadening results mainly from grain refinement after SMAT. The broadening of the half-height of the diffraction peak is inversely proportional to the lattice size. Therefore, the increase in half-height width indicates that mechanical grinding treatment can reduce the grain size significantly. The average grain size of the Ta, Ta_{SMAT2}, and Ta_{SMAT5} samples was 73.8, 37.1, and 13.2 nm, respectively, as calculated by the Scherrer formula [12], which indicates that the grain size on the specimen surface was reduced significantly and the grain boundary concentration increased after SMAT.

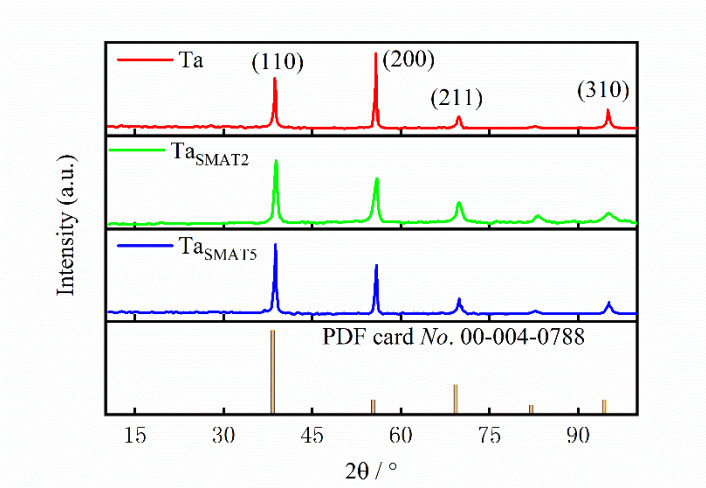

Figure 3. XRD analysis of Ta before and after SMAT. Test parameters: the phase compositions and average crystallite sizes were determined by XRD with Cu–Kα radiation (tube voltage: 40 kV, tube current: 200 mA for structural analysis). XRD analysis was performed with a scanning speed of 1°/min and a 2θ range of 10–100° for wide-angle XRD patterns.

3.2 Depth sputtering analysis of Ta anodic oxide coating

After anodizing, the oxide film layer thickness was assessed by XPS depth sputtering. The depth sputtering diagrams before and after SMAT are shown in Fig. 4, where the atomic percentage of elemental O was used as a criterion for the disappearance of the oxide film. The oxide film thickness of Ta was ~200 nm, and when the depth of the Ta_{SMAT2} and Ta_{SMAT5} specimens reached 462 and 880 nm, respectively, the surface of the Ta_{SMAT2} and Ta_{SMAT5} specimens had zero percent elemental O, which indicates that the oxide film layer thickness increased by 131% and 340% after SMAT. The results imply that SMAT contributes to the oxide film growth.

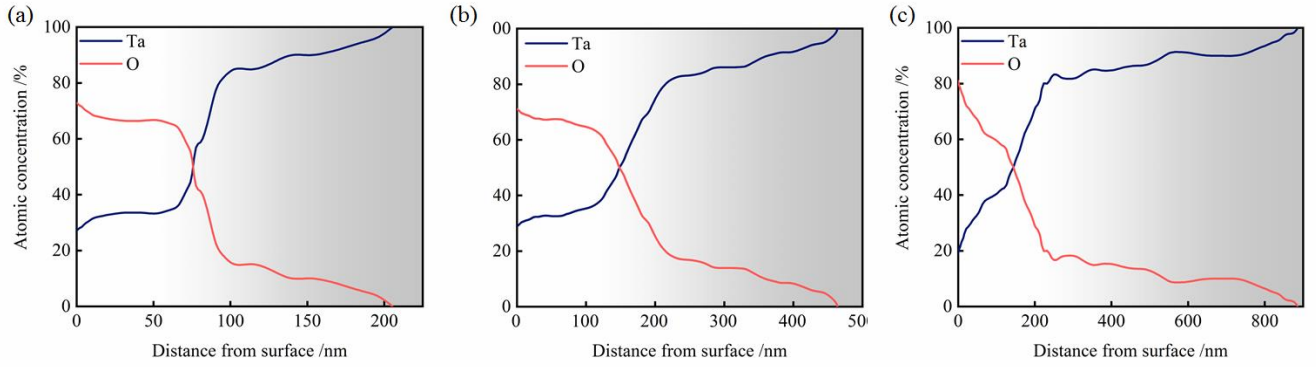

Figure 4. XPS analysis of thickness of mechanically ground Ta anodic oxide film (a) Ta, (b) Ta_{SMAT2}, (c) Ta_{SMAT5} . A 4 × 4 mm^2 area of the surface oxide film was sputtered using an Ar^+ beam by multifunctional X-ray photoelectron spectroscope (PHI5000 Versaprobe-II).

3.3 Electrochemical properties of Ta anodic oxide coating

The electrochemical properties were investigated to assess the effect of SMAT on the corrosion performance of the Ta surfaces. A higher corrosion potential implies less corrosion, whereas a lower corrosion current implies a slower corrosion rate. Figure 5 shows the potentiodynamic polarization curves before and after SMAT. The corrosion potential (E_{corr}) of Ta_{SMAT5} was –1.143 V_{SCE} whereas the E_{corr} of Ta_{SMAT2} and Ta was –1.206 V_{SCE} and –1.297 V_{SCE}, respectively. Ta_{SMAT5} had the lowest corrosion current (1.028 × 10^{-4} A·cm^{-2}) compared with Ta (2.618 × 10^{-4} A·cm^{-2}) and Ta_{SMAT2} (2.334 × 10^{-4} A·cm^{-2}) samples. The SMAT can increase the corrosive potential and reduce the corrosion current, which implies that the anodic oxide film that was produced after SMAT had a better corrosion resistance.

After a short period of dissolution, the polarization curve of the SMAT samples showed typical passivation characteristics in the range of corrosion potentials from –0.3 to 1.0 V_{SCE}, with a passivation zone of a dimensional passivation current density of ~0.3 mA·cm^{-2}. Passivation was caused by the formation of a dense oxide film on the Ta surface, which prevents the corrosion reaction from occurring.

At the E = 0.0 V_{SCE} position, an increase in current density occurs in the sample specimen. According to Oliveira et al. [13], the increase in current density in the kinetic potential polarization curve reflects oxide film rupture, and the subsequent decrease in current density reflects the occurrence of repassivation on the sample surface. The current density of the dimensional passivation after

repassivation is higher than that of the first passivation and increases slowly with current density. After repassivation the current density was higher than that of the first passivation and increased slowly with an increase in voltage, which indicates that the newly generated oxide film was not as dense as the original oxide film. The oxide film of the Ta_{SMAT2} and Ta_{SMAT5} sample remained stable during the kinetic potential polarization curve, and the j_{corr} of the Ta_{SMAT5} and Ta_{SMAT2} sample was approximately half an order of magnitude lower than that of the Ta sample, which reflects the excellent stability of the Ta_{SMAT5} and Ta_{SMAT2} sample in the corrosive medium.

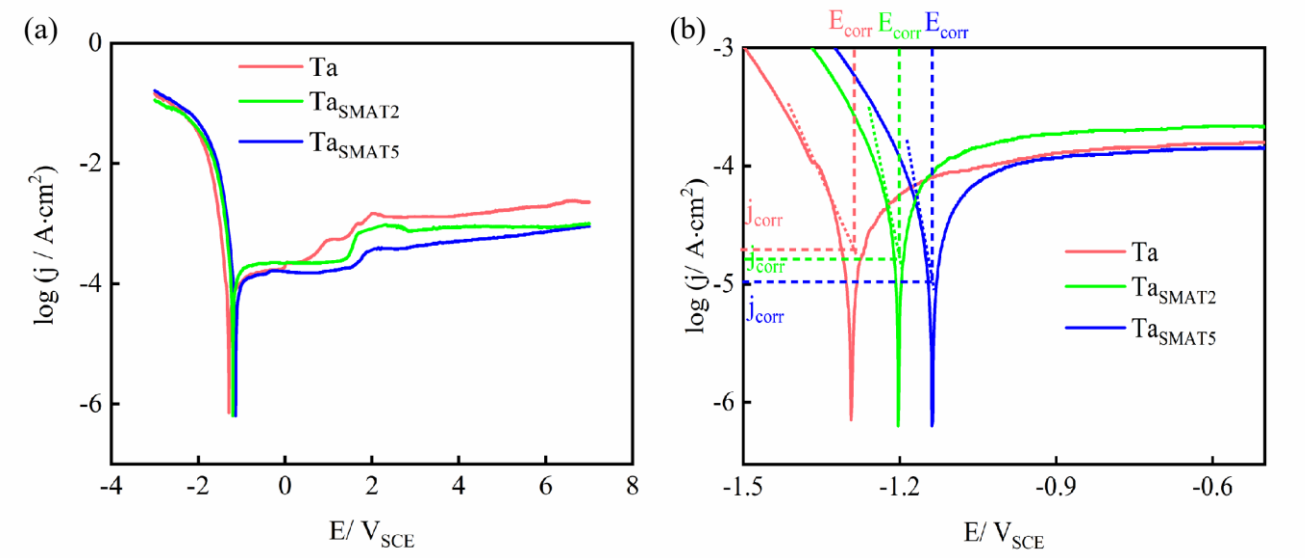

Figure 5. Potentiodynamic polarization curves analysis of Ta anodic oxide film (a) Potentiodynamic polarization curves (b) Enlarged view of Tafel area.

The effect of SMAT on the oxide film on the Ta surface was investigated by using electro-impedance spectroscopy (EIS). Figure 6a–b shows the Nyquist plot and Bode plot in a 3.5 wt.% NaCl solution, respectively. One of the Nyquist plots has an incomplete capacitance arc. The size of the diameter of the capacitive arc indicated that a longer mechanical grinding time contributed to the corrosion resistance. The Bode diagram shows that the mechanically ground sample had a capacitive resistance behavior, with a phase angle peak in the range of 10^0–10^3 Hz. The phase angle peak was less than 90°, which indicates that the oxide film does not exhibit the desired capacitive behavior. As the mechanical grinding treatment time increased, the maximum phase angle peak approached 90°. A wider range of maximum value maintained a phase angle that was closer to the electrochemical response characteristics of the ideal capacitance. This result suggests that the SMAT helps to improve the oxide film stability, reduces charge transport, and provides an excellent barrier to Cl^- penetration [14].

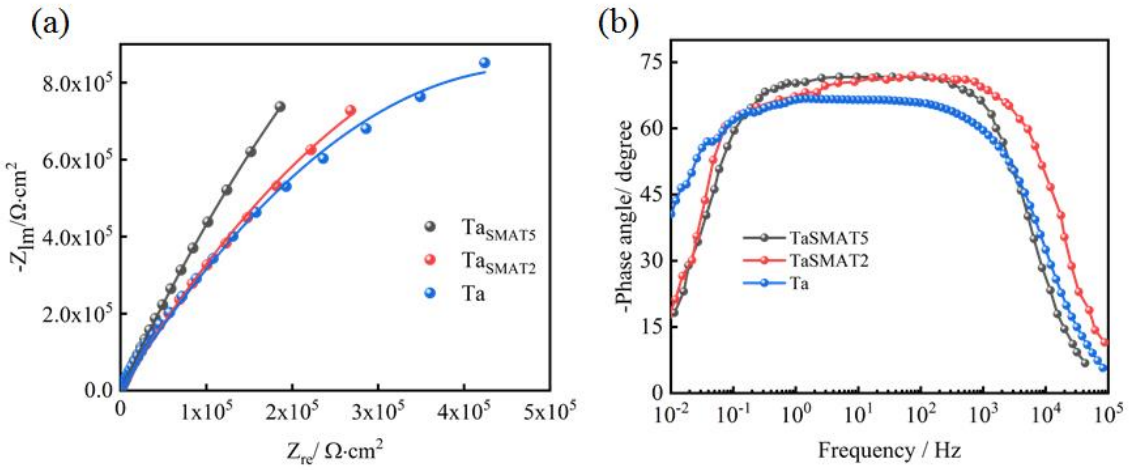

Figure 6. Impedance analysis of Ta anodic oxide film (a) Nyquist plot and (b) Bode plot

The fitted circuit was used to investigate the corrosion resistance of the film layer. The anodic oxide surface model is shown in Fig. 7a with the presence of an oxide film pore layer on its surface and a dense oxide layer and substrate beneath. Therefore, the undesirable capacitance was replaced by the equivalent original (CPE) in its fitted circuit, whose value can be obtained by:

$$Z_{CPE}(\omega)=\frac{1}{Q(j\omega)^{\alpha}} \quad (1)$$

where CPE is a constant, ω is the angular frequency (rad/s), $j^2 = -1$, and α is the latitudinal coefficient ($0 < a < 1$).

Combined with the membrane layer structure, the equivalent circuit in this paper is shown in Fig. 7b. It is composed of the following components: R_s represents the solution resistance, R_1 represents the resistance of the outer porous layer, CPE_1 represents the capacitance of the outer porous layer, R_2 represents the resistance of the inner dense layer, and CPE_2 represents the capacitance of the inner dense layer. The accuracy of the fit was evaluated by using the chi-square coefficient χ^2. The results showed that the χ^2 of all three samples was less than 10^{-3}, which indicates that the fitted results and the experimental curves have a relatively good reproducibility. The fitting results are shown in Table 1.

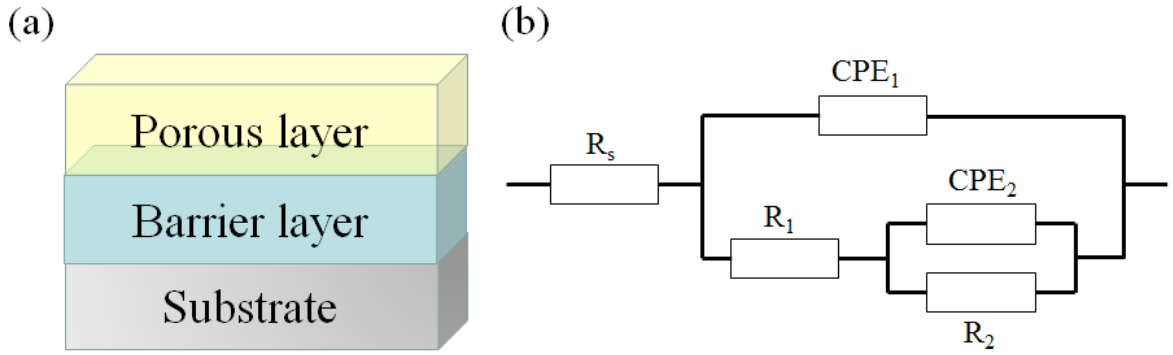

Figure 7. Passive film model and equivalent circuit used for fitting EIS (a) passive film model, (b) equivalent circuit

Table 1 shows that the R_1 value of the Ta_{SMAT5} sample is largest at 17.930 kΩ·cm^2, followed by the Ta_{SMAT2} sample at 13.271 kΩ·cm^2, and the lowest was for the Ta sample at ~6.822 kΩ·cm^2. R_1 reflects the diffusion of corrosive media in the porous layer. A larger R_1 indicates a decrease in porosity of the porous layer and an increase in the diffusion path of the corrosive medium in the porous layer. R_2 is the dense layer resistance, and its value exceeds that of R_1, which indicates that the dense layer, because of the compact structure of the oxide film, inhibits Cl^- diffusion, and the dense layer has a greater effect on the corrosion resistance. With an increase in grinding time, the value of R_2 increased gradually. The Ta_{SMAT5} sample had the largest R_2 of 32.219 kΩ·cm^2, followed by the Ta_{SMAT2} sample at 21.847 kΩ·cm^2 and the lowest was the Ta sample at ~16.283 kΩ·cm^2. The increase in potential reduces the porosity of the outer layer, and improves the inner-layer density.

Table 1. Fitting data of EIS for Ta_{SMAT5}, Ta_{SMAT2}, and Ta

Samples	CPE_1 (μF.cm^{-2})	α_1	CPE_2 (μF.cm^{-2})	α_2	R_s （Ω.cm^2）	R_1 （kΩ.cm^2）	R_2 （kΩ.cm^2）	χ^2（10^{-4} ）
Ta	0.01386	0.844	1.716	0.597	1.123	6.822	16.283	7.104
Ta_{SMAT2}	0.00898	0.739	1.465	0.642	1.108	13.271	21.847	8.463
Ta_{SMAT5}	0.00416	0.891	1.168	0.681	1.126	17.930	32.219	5.278

3.4 Molecular dynamics analysis of Ta anodic oxide coating

To elucidate the activation mechanism of the Ta surface by surface mechanical grinding, the surface state after surface mechanical grinding was simulated by using molecular dynamics. Models with different grain numbers in a 100 nm ×100 nm ×100 nm box are shown in Fig. 8a, where the blue region is the body-centered cubic crystal structure, whereas the other colored regions are the face-centered cubic or hexagonal close-packed crystal structures. As the grain number increases, the proportion of other non-stationary structures increases and is concentrated mainly at the grain boundaries, which implies that the energy at the grain boundaries is elevated compared to within the grain.

The surface energy of the three structures after sectioning is shown in Fig. 8b. The surface energy is defined as $E_{surface} = (E_{after} - E_{before})/(2A)$, where E_{before} and E_{after} are the energies of the faceted surface and A is the cross-sectional area, respectively. As the number of grains increases, the surface energy of the material increases, and reaches 2.399 J/m^2 when the number of grains reaches 10, which represents an energy increase of 14.840% over that of one grain. According to Yu [15], a higher material surface energy yields a higher surface activity. Therefore, when the material is ground mechanically on the surface, the material surface grain size decreases and the interfacial concentration increases, which leads to an increase in activity, and the interfacial sites provide nucleation sites for nucleation of the surface film layer, which is consistent with the experimental results of Azadmanjiri [16].

The mean square displacement of the material at 300 K was analyzed as shown in Fig. 8c. The slope of the mean square displacement is the diffusion coefficient of the Ta atoms, and a larger slope implies a larger diffusion coefficient. The slope of the root-mean-square displacement of the material increased significantly with an increase in grain number. Further calculations of the diffusion number rates for the three structures show that the atomic diffusion rates were 1.371×10^{-6} m^2/s, 9.230×10^{-5} m^2/s, and 5.126×10^{-4} m^2/s for grains 1, 5, and 10, respectively, with the diffusion rate for grain 10 being 374 times higher than the diffusion rate for grain 1. According to the point defect model principle [17], the formation of oxide layers is a combination of outward diffusion of metal atoms and inward diffusion of oxygen atoms. The interface provides an ideal channel for atomic interdiffusion, which promotes film layer thickening and enhances the corrosion resistance.

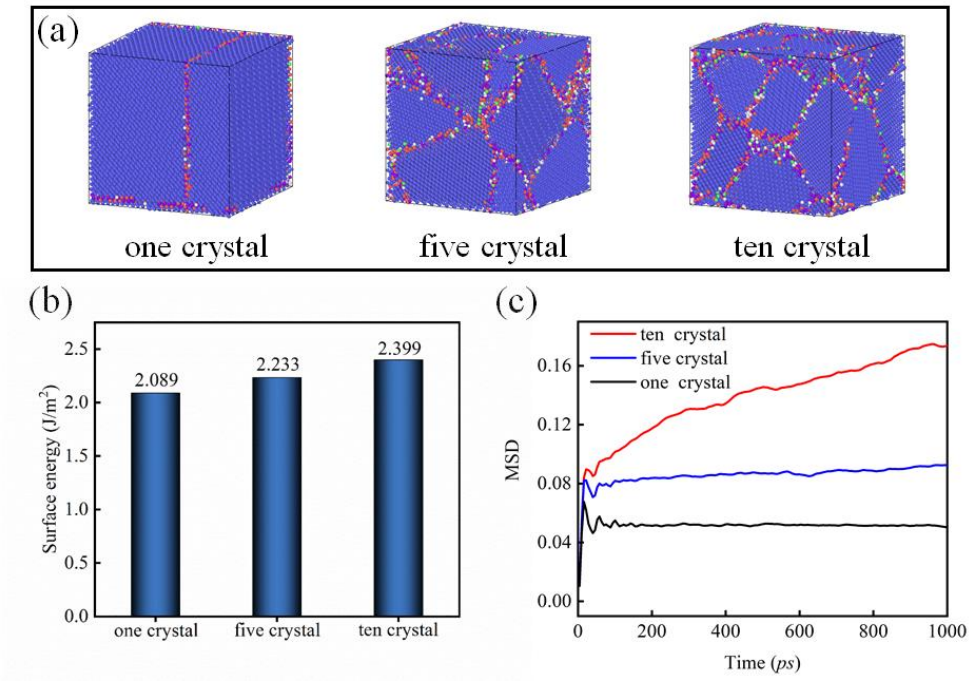

Figure 8. Molecular kinetic analysis of SMAT promotion of oxide film production (a) nanocrystalline structures. The blue region is the body-centered cubic crystal structure, whereas the other colored regions are the face-centered cubic or hexagonal close-packed crystal structures. (b) surface energy, (c) mean square displacement.

4. CONCLUSIONS

Mechanical grinding was used to enhance the corrosion resistance of the Ta surfaces. The average grain size of the Ta and Ta_{SMAT5} samples was 73.8 nm and 13.2 nm, respectively, which indicates that the grain size on the specimen surface was reduced significantly and the grain boundary concentration increased after mechanical grinding pretreatment. XPS depth sputtering showed that the oxide film layer was enhanced by 340% after SMAT. The electrochemical properties of the Ta anodic oxide coating showed that the SMAT increased the corrosive potential (–0.1.143 V_{SCE} of Ta_{SMAT5}) and reduced the corrosion current (1.028×10^{-4} $A\cdot cm^{-2}$ of Ta_{SMAT5}), which implies that the anodic oxide film that was

produced after SMAT exhibited a better corrosion resistance. The diffusion number rates for the three structures showed that the atomic diffusion rates were 1.371×10^{-6} m^2/s, 9.230×10^{-5} m^2/s, and 5.126×10^{-4} m^2/s for grains 1, 5, and 10, respectively. The interface provided the ideal channel for atomic interdiffusion, which promoted the thickening of the film layer and enhanced the corrosion resistance. In this study, a method of SMAT followed by anodic oxidation was proposed, which can improve the corrosion resistance of Ta surfaces.

ACKNOWLEDGEMENTS
We are grateful for financial support from the Scientific Research Fund of Yunnan Education Department (grant nos. 2020J0054, 2020J0416 and 2019J0039), the National Nature Science Foundation of China (grant nos. 52061019), the Key Projects of Basic Research Plan of Yunnan Science and Technology Department (grant nos. 202001AS070048), the Major Science and Technology Program of Yunnan Province (202002AB080001-1), the Key Projects of the Yunnan Basic Research Program (2019FA048), and the General Projects of the Basic Research Plan of Yunnan Science and Technology Department (grant nos. 202001AT070147).

References

1. A.Persdotter, T. Boll and T. Jonsson, *Corros. Sci.*, 192 (2021) 109779.
2. D.L. Zhao, C.J. Han, Y. Li, J.J. Li, K. Zhou, Q.S. Wei, J. Liu and Y.S. Shi, *J. Alloy. Compd.*, 804 (2019) 288.
3. A.C. Hee, S.S. Jamali, A. Bendavid, P.J. Martin, C.L. Kong and Y. Zhao, *Surf. Coat. Tech.*, 307 (2016) 666.
4. G. Amsel, C. Cherki, G. Feuillade and J.P. Nadai, *J. Phys. Chem. Solids*, 30 (1969) 2117.
5. W. Hu, J. Xu, X.L. Lu, D.S. Hu, H.L. Tao, P. Munroe and Z.H. Xie, *Appl. Surf. Sci.*, 368 (2016) 177.
6. Y. Li, T.T. Zhao, S.B. Wei, Y. Xiang and H. Chen, *Mat. Sci. Eng. C*, 30 (2010) 1227.
7. R. Vallat, R. Gassilloud, B. Eychenne and C. Vallee, *J. Vac. Sci. Technol. A*, 35 (2017) 01B104.
8. T.L. Fu, Z.L. Zhan, L. Zhang, Y.R. Yang, Z. Liu, J.X. Liu, L. Li and X.H. Yu, *Surf. Coat. Tech.*, 280 (2015) 129.
9. X. Wang, X.H. Yu, J. Rong, X.Y. Li, Y. Zhong, J. Feng and Z.L. Zhan, *Mater. Res. Express*, 5 (2018) 095010.
10. Y.H. Li, D.J. Siegel, J.B. Adams and X.Y. Liu, *Phys. Rev. B*, 67 (2003) 125101.
11. K. Lu, J. Lv, *J. Mater. Sci. Tech.,* 15 (1999) 193.
12. A.L. Patterson, *Phys. Rev.*, 56 (1939) 978.
13. N.T. Oliveira and A.C. Guastaldi, *Acta Biomater.*, 5 (2009) 399.
14. T. Balusamy, T.S.N. Sankara Narayanan, K. Ravichandran, S. Park and M. H. Lee, *Corros. Sci.*, 74 (2013) 332.
15. N.F. Yu, N. Tian, Z.Y. Zhou, L. Huang, J. Xiao, Y.H. Wen and S.G. Sun, *Angew. Chem. Int. Edit.*, 53 (2014) 5097.
16. J. Azadmanjiri, C.C. Berndt, A. Kapoor and C. Wen, *Crit. Rev. Solid State*, 40 (2015) 164.
17. D.D. Macdonald, *Electrochim. Acta*, 56 (2011) 1761.